Article

Workability of Nanomodified Self-Compacting Geopolymer Concrete Based on Response Surface Method

Yong-Hua Tian [1], Jia-Cheng Tao [2,3], Tao Luo [2,3] and Li Li [2,3,*]

1   Sinohydro Fifth Engineering Bureau Limited, Chengdu 610066, China
2   Key Laboratory of Agricultural Soil and Water Engineering in Arid and Semiarid Areas of Ministry of Education, Northwest A&F University, Yangling 712100, China
3   College of Water Resources and Architectural Engineering, Northwest A&F University, Yangling 712100, China
*   Correspondence: drlili@nwafu.edu.cn

Abstract: Geopolymer concrete is more low-carbon and environmentally friendly than Portland cement concrete. Nanoparticle modification can help to improve the mechanical and durability performance of concrete, but due to its large specific surface area and high activity, it may deteriorate its workability. However, there is currently limited research on the effect of nanomodification on the workability of freshly mixed self-compacting geopolymer concrete (SCGC). This article conducted SCGC workability experiments using the response surface methodology, which included 29 different mixtures. The effects of nano-silica (NS), nano-calcium carbonate (NC), alkali content (N/B), and water cement ratio (W/B) on the workability of SCGC were studied. The experimental results show that the addition of NS and NC can reduce the slump expansion of SCGC, and the combination of the two significantly increases the amplitude of slump expansion with the change in nanomaterial content. An increase in N/B will reduce the expansion time and clearance value of SCGC. As N/B increases from 4% to 4.4%, the slump extension of SCGC decreases, and with a further increase in N/B, the slump extension increases significantly to 68.1 cm, which means that the slump extension of SCGC increases by 9.5% as N/B increases from 4.4 to 5. This study can provide a reference for optimizing the fresh performance of geopolymer concrete and improving the mechanism of nanomaterial-modified geopolymer concrete.

Keywords: self-compacting geopolymer concrete (SCGC); response surface method; working performance; modification of nanomaterials

1. Introduction

Concrete is currently the most widely used and makes up the largest amount of produced construction materials; in recent years, the annual production of concrete worldwide reached more than 5 billion tons, which means that a large amount of cement is also consumed at the same time. The production of cement emits CO_2 of equal mass; for one ton of cement produced, approximately one ton of CO_2 is also emitted [1]. These CO_2 emissions accompanying the production of cement account for about 7–8% of global CO_2 emissions, which are constantly exacerbating the Earth's greenhouse effect. In addition, China's coal, mineral, and other resource consumption is huge; in 2021, China's general industrial solid waste generation reached up to 3.6 billion tons, yet the overall utilization rate of industrial solid waste was still less than 60%. There is an urgent need to improve the comprehensive utilization rate of solid waste in order to achieve development goals, such as energy saving and emission reduction in solid waste utilization. Recently, geopolymer concrete has become an alternative to ordinary Portland concrete (OPC) as an environmentally friendly material [2–4]. Unlike OPCs, geopolymers are formed by the alkali excitation of alumino-silicate minerals, which are composed of fly ash (FA), blast furnace slag (BFS), and other industrial by-products [5], and have high compressive strength [6], freeze–thaw

resistance [6], high temperature resistance [7], and acid resistance [8]. The production of geopolymers is characterized by low carbon emissions and low energy consumption, as well as the consumption of industrial by-products FA and construction waste. Therefore, geopolymer is a green material with a wide range of applications in civil engineering [9,10].

Self-compacting concrete (SCC) is typically characterized by large flowability, good fillability, and high throughput capacity without segregation or water seepage, making it particularly suitable for use in precast elements, high-rise buildings and structures requiring dense reinforcement. Conversely, self-compacting geopolymer concrete (SCGC) is a new concept in the field of concrete and is an advanced type of concrete that possesses the properties of both geopolymer concrete and SCC. However, geopolymer concretes are more complex than OPC concretes due to the complexity of their proportioning and precursor chemical–physical properties, leading to more complex workability regulation than OPC concretes. In addition, most of the high-efficiency water-reducing agents such as polycarboxylic acid, which are commonly used in OPC concretes, are ineffective in geopolymer concretes for the regulation of fluidity [11]. An unstable working performance and the difficulty to regulate it are also one of the important reasons hindering the large-scale application of SCGC.

In recent years, the application of nanomaterials in concrete has received much attention [12–15], and nano-silica (NS) is one of the most widely researched nanomaterials [16]; it exhibits the filling effect [17], the surface effect [18], the nucleation effect, and the volcanic ash effect [16]. Studies have shown that the addition of NS can significantly increase the compressive, flexural, and tensile strength of concrete [19], and plays a significant role in reducing the porosity and water absorption of concrete, improving the microstructure and durability properties [20]. Although the activity of nano-calcium carbonate (NC) is on the low side compared to NS, its price is only one-tenth of that of NS, making it the least expensive of the common nanomaterials. In addition, NC improves the microfine particle gradation, reduces stacking voids, and reinforces the microaggregate effect, which helps to improve the workability of concrete. In addition, geopolymer cementitious materials have a more highly alkaline liquid phase environment that is significantly different from that of OPC cementitious materials, and reaction products that are different from those of OPC systems, such as C-A-S-H, N-A-S-H, and hydrotalcite phases. The studies that have been conducted on nanomodified geopolymer materials have focused on their positive effects on the mechanical and durability properties of concrete, as well as on the bonding properties of the fiber–concrete interface [21–23]. However, there are fewer studies on the effect of NC on the fresh properties of geopolymer concrete, and there is a lack of literature on the composite modification of geopolymer concrete by NC and NS. Therefore, exploring the effect of NS and NC composite modification on the working performance of SCGC is of great significance to enhance the material performance, extend its application range, and promote the development and scale-up of geopolymer, a low-carbon building material.

In this study, based on the response surface methodology for designing the proportioning, a four-factor, three-level test was carried out with the water/binder ratio (W/B), alkali content (N/B), NS doping, and NC doping as variables to test the workability of freshly mixed SCGCs, and the results were analyzed using Design Expert software to quantitatively evaluate the effects of nanomaterials doping, W/B, and N/B on the workability of the BFS-FA composite excitation system SCGC. The influencing factors were optimally selected and subjected to micro-morphological observation and mechanism analysis. It is conducive to the reduction in cost, energy consumption, and the promotion of environmental protection, provides reference for the formulation of nanomodified SCGC and the construction of related projects, and is of great practical significance for the sustainable development of the concrete industry.

2. Experiment Program

2.1. Raw Materials and Preparation of SCGC

The FA (class F) used in this experiment was from Weihe Power Plant (Xianyang, China). The BFS was made of Shaanxi Delong (Xianyang, China) S95 granulated blast furnace slag powder with a density of 2.8 g/cm^3, a specific surface area of 422 m^2/kg, an alkalinity coefficient of 0.30, and an activity coefficient of 0.96. NS and NC were provided by Shanghai Maclean's Biochemical Technology Co (Shanghai, China). The NS had a density of 2.6 g/mL at 25 °C and a measured pH of 5.5. The nano-silica appeared as an amorphous white powder, with a particle size range of 1–100 nm, a spherical microstructure, a flocculent and reticulate quasiparticle structure, and a small size effect and surface effect. The purity of NC was 95.1%. The chemical compositions of BFS, FA, NS, and NC, as determined by X-ray fluorescence (XRF), are shown in Table 1. It can be seen that BFS is composed mainly of silica and calcium oxide and FA is composed mainly of silica and alumina, with NS containing about 98% silica and NC containing about 94% calcium oxide. Figure 1 illustrates the SEM images of the gelling material and the nanomodified material, where it can be observed that the BFS has an irregular shape and the FA is an inhomogeneous spherical particle containing different sizes (some of which are hollow). The physical properties of BFS, FA, NS, and NC are listed in Table 2.

Table 1. Chemical composition of BFS, FA, NS, and NC (% by mass).

Constituents	BFS	FA	NS	NC
SiO_2	35.08	52.84	97.85	1.01
CaO	35.48	5.97	0.14	93.82
Al_2O_3	14.92	25.65	0.55	0.21
SO_3	2.35	2.61	-	0.13
Na_2O	1.36	1.49	0.24	0.12
Fe_2O_3	0.92	6.07	0.09	0.06
MgO	7.52	1.1	-	4.5
K_2O	0.49	1.72	0.11	-

Figure 1. The schematic diagram of SCGC preparation process.

Table 2. Physical properties of BFS, FA, NS, and NC.

Properties	BFS	FA	NS	NC
Material type	Gelling	Gelling	Nanomodified	Nanomodified
Median particle size	7.9 μm	7.1 μm	677 nm	375 nm
Material characteristics	Volcanic ash reactivity, Microaggregate effect, Microcrystalline nucleation effect	Porous honeycomb organization, High adsorption activity	Flocculated and reticulated particle structure, Small size effect, Surface effect	Surface effects, Quantum size effects, Macroscopic quantum tunneling effects

It should be noted that NS particles are irregular in shape and have a rougher surface, while NC particles are smaller and have a spherical surface. The size of the nanoparticles is much smaller than that of cementitious materials; specifically, the average particle sizes of fly ash and slag are about 20 μm and 10 μm, respectively, while the average particle sizes of NS and NC are about 0.7 μm and 0.4 μm, respectively, which is two orders of magnitude different.

Intermediate sand with a fineness modulus of 2.8 was used; Weihe River sand was used as fine aggregate, and pebbles of 5–12 mm continuous grading were used for coarse aggregate. The alkaline exciter was sodium hydroxide (NaOH) powder mixed with sodium silicate solution to a modulus ($M = n(SiO_2)/n(Na_2O)$) of 1.24. The sodium silicate solution had a Baume, density, and modulus of 40, 1.38 g/cm^3, and 3.22, respectively.

2.2. RSM Design and Proportioning

The RSM function of the Design Expert software developed by Stat-ease was used for the design of the rationing of the independent variables. Response surface modeling pairs input factors (independent variables) in order to better analyze the effects of their interactions on the dependent variable (response), where different combinations of three levels of four variables (N/B, W/B, NS doping, and NC doping) were considered. These four variables varied from 4% to 5% for N/B, 0.5 to 0.6 for W/B, 0 to 0.4% for NS doping, and 0 to 0.4% for NC doping. The Box–Behnken response surface method [24] was used to obtain 29 groups of fits, as shown in Table 3, in order to minimize the factors affecting the variations; the amounts of cementitious materials, aggregates, and water glass were kept the same for the different proportioning groups, and the variations in N/B were adjusted by mixing sodium carbonate powder. The responses of interest in this study are the work performance metrics such as the slump extensibility, the expansion time for expansion diameters up to 500 mm (T500), and the gap passage value of the SCGC.

Table 3. Mix proportions of SCGC.

	FA (kg/m^3)	BFS (kg/m^3)	Coarse Aggregate (kg/m^3)	Fine Aggregate (kg/m^3)	Water (kg/m^3)	Activators (kg/m^3)	Na2CO3 (kg/m^3)	NS (kg/m^3)	NC (kg/m^3)
1	225	225	371.4	432.8	214.6	91	0	0.9	0.9
2	225	225	371.4	432.8	214.6	91	7.7	0.9	0.9
3	225	225	371.4	432.8	259.6	91	0	0.9	0.9
4	225	225	371.4	432.8	259.6	91	7.7	0.9	0.9
5	225	225	371.4	432.8	237.1	91	3.8	0	0
6	225	225	371.4	432.8	237.1	91	3.8	1.8	0
7	225	225	371.4	432.8	237.1	91	3.8	0	1.8
8	225	225	371.4	432.8	237.1	91	3.8	1.8	1.8
9	225	225	371.4	432.8	237.1	91	0	0.9	0
10	225	225	371.4	432.8	237.1	91	7.7	0.9	0
11	225	225	371.4	432.8	237.1	91	0	0.9	1.8
12	225	225	371.4	432.8	237.1	91	7.7	0.9	1.8
13	225	225	371.4	432.8	214.6	91	3.8	0	0.9
14	225	225	371.4	432.8	259.6	91	3.8	0	0.9
15	225	225	371.4	432.8	214.6	91	3.8	1.8	0.9
16	225	225	371.4	432.8	259.6	91	3.8	1.8	0.9
17	225	225	371.4	432.8	237.1	91	0	0	0.9
18	225	225	371.4	432.8	237.1	91	7.7	0	0.9
19	225	225	371.4	432.8	237.1	91	0	1.8	0.9
20	225	225	371.4	432.8	237.1	91	7.7	1.8	0.9
21	225	225	371.4	432.8	214.6	91	3.8	0.9	0
22	225	225	371.4	432.8	259.6	91	3.8	0.9	0
23	225	225	371.4	432.8	214.6	91	3.8	0.9	1.8
24	225	225	371.4	432.8	259.6	91	3.8	0.9	1.8
25	225	225	371.4	432.8	237.1	91	3.8	0.9	0.9
26	225	225	371.4	432.8	237.1	91	3.8	0.9	0.9
27	225	225	371.4	432.8	237.1	91	3.8	0.9	0.9
28	225	225	371.4	432.8	237.1	91	3.8	0.9	0.9
29	225	225	371.4	432.8	237.1	91	3.8	0.9	0.9

2.3. Mixing Procedures and Test Methods

2.3.1. Mixing Program

Nanomaterials are very easy to agglomerate, which affects their modification effect on SCGC. In this experiment, NS and NC were pre-dispersed mechanically. NS was first added to water and then stirred at high speed for 3 min with a hand-held micro-stirrer, and the state of dispersion was significantly improved after stirring. The schematic diagram of the SCGC preparation process is shown in Figure 1.

The mixing process starts by dry mixing the cementitious materials with sand and gravel aggregates and sodium carbonate powder in a concrete mixer for 60 s. The water glass solution and water are poured into the mixer, and the nanomaterials are poured in after mixing for 120 s. After this, the freshly mixed SCGCs are obtained by mixing for 300 s.

2.3.2. Workability Test

The workability test of freshly mixed SCGC was carried out, including the three aspects of fluidity, flow rate, and gap passage, and the photographs during the testing process of three specific indexes, namely slump spread, T500, and gap passage value, are shown in Figure 2. The test methods and requirements were completed in accordance with the standard JGJ/T283-2012 "Application of Self-Compacting Concrete Technical Specification" [25]. For the test using the slump cylinder and non-absorbent platform, the latter with an area of more than 700 mm^2 (flow bench), two concentric circles were marked on the flow bench, with the center position marking the slump cylinder placed in the center position; the marking at the diameter of 500 mm was used for the determination of T500. A slump cylinder placed on the center circle was filled with freshly mixed concrete and then lifted to allow the free flow of SCGC on the flow bench. The time from the lifting of the slump cylinder until the diameter of the extended surface of the slump of the mix reaches 500 mm is recorded as T500, in s. As shown in Figure 2a, after the flow of the mixture was stopped, the average value of the maximum diameter of the slump spread surface and the diameter in the perpendicular direction to the maximum diameter were measured using a tape measure to obtain the slump spread degree in cm. As shown in Figure 2b, the J-ring is placed on the concentric circle position of the slump cylinder, and after the flow of the mixture stops, the J-ring extensibility is obtained by using a tape measure to measure the average of the maximum diameter of the extended surface of the J-ring and the diameter in the perpendicular direction to the maximum diameter, in cm. The difference between the slump extensibility and the J-ring extensibility was applied as the gap passage value to reflect the gap passage of the SCGC.
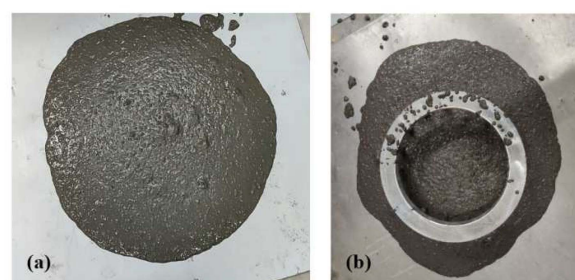

Figure 2. Workability test. (**a**) Slump spread test, (**b**) J-ring extensibility test.

3. Response Surface Modeling Analysis

3.1. Modeling Equations

The response values for this test were slump spread, T500, and gap passage values, and the independent variables were N/B, W/B, NS doping, and NC doping, represented by A, B, C, and D, respectively, with low, medium, and high test levels coded as −1, 0, and 1 for each independent variable, respectively (see Table 4).

Table 4. Test factor levels and coding.

Factor	Code	Level		
		−1	**0**	**1**
N/B (%)	A	4.0	4.5	5.0
W/B	B	0.50	0.55	0.60
NS (wt.%)	C	0	0.2	0.4
NC (wt.%)	D	0	0.2	0.4

Let the quadratic polynomial equation fitted to this model by least squares be

$$\check{Y} = c_0 + \sum_{i=1}^{n} a_i x_i + \sum_{j \leq i}^{n} b_{ij} x_i x_j \tag{1}$$

where Y is the predicted response value, the predicted value of the workability indicator x_i and x_j are the coded values of the independent variables, c_0 is the constant term, a_i is the linear coefficient, b_{ij} is the quadratic term coefficient, and n is the number of factors, which is four in this experiment.

The results of the response factors obtained from the test are shown in Table 5, and the coefficients in Equation (1) were fitted by regression using the test results as input factors in accordance with the statistical requirements of the Box–Behnken experimental design. Quadratic multinomial regression equations were obtained for the slump extensibility, T500, and gap passage values of SCGC on the coded independent variables N/B, W/B, NS doping, and NC doping:

$$\text{Slump spread} = +460 - 203A + 125B - 307D - 28C - 65AB + 29AD - 15AC + 263BD + 88BC + 19CD + 26A^2 + 268B^2 + 101C^2 + 71D^2 \tag{2}$$

$$\text{T}_{500} = +269 - 22A - 760B + 10C + 73D + 39AB - 1.4AD + 2.6A\,C - 113BD - 17BC - 0.6CD - 0.1A^2 + 508B^2 - 31C^2 - 7D^2 \tag{3}$$

$$\text{Gap passing value} = -37 + 6.6A + 90B + 165D - 63C - 15AB - 7.5AD + 12AC - 250BD - 2.5BC + 25CD \tag{4}$$

Table 5. Box–Behnken response surface method design program and results for each response factor.

	Factors				Responses		
	N/B (kg/m³)	W/B (kg/m³)	NS (wt.%)	NC (wt.%)	Slump Expansion (cm)	T500 (s)	Gap Passing Value (cm)
1	4.0	0.50	0.2	0.2	51.5	10.9	5.5
2	5.0	0.50	0.2	0.2	59.5	6.0	6.0
3	4.0	0.60	0.2	0.2	81.5	2.2	1.5
4	5.0	0.60	0.2	0.2	83.0	1.2	0.5
5	4.5	0.55	0	0	71.5	2.0	6.0
6	4.5	0.55	0.4	0	66.0	2.0	3.0
7	4.5	0.55	0	0.4	69.5	2.7	0.5
8	4.5	0.55	0.4	0.4	67.0	2.7	1.5
9	4.0	0.55	0.2	0	74.5	2.0	2.5
10	5.0	0.55	0.2	0	64.5	2.2	3.5
11	4.0	0.55	0.2	0.4	69.0	2.1	5.0
12	5.0	0.55	0.2	0.4	70.5	1.8	3.0
13	4.5	0.50	0	0.2	60.5	3.1	4.5
14	4.5	0.60	0	0.2	69.5	0.9	0.5
15	4.5	0.50	0.4	0.2	58.5	4.2	5.5
16	4.5	0.60	0.4	0.2	71.0	1.3	1.5
17	4.0	0.55	0	0.2	67.5	2.0	8.0
18	5.0	0.55	0	0.2	74.5	1.5	4.0
19	4.0	0.55	0.4	0.2	70.5	1.1	0.5
20	5.0	0.55	0.4	0.2	71.5	1.6	1.3

Table 5. *Cont*.

Factors				Responses		
N/B (kg/m^3)	W/B (kg/m^3)	NS (wt.%)	NC (wt.%)	Slump Expansion (cm)	T500 (s)	Gap Passing Value (cm)
21	4.5	0.50	0.2	0	56.0	4.5	2.0
22	4.5	0.60	0.2	0	72.5	0.9	7.5
23	4.5	0.50	0.2	0.4	50.0	8.9	8.5
24	4.5	0.60	0.2	0.4	77.0	0.9	4.0
25	4.5	0.55	0.2	0.2	56.5	3.9	4.5
26	4.5	0.55	0.2	0.2	59.0	3.8	1.0
27	4.5	0.55	0.2	0.2	63.0	3.0	1.8
28	4.5	0.55	0.2	0.2	63.0	2.5	0.5
29	4.5	0.55	0.2	0.2	62.0	1.9	4.0

3.2. Significance Test

Table 6 shows the model validation parameters. The accuracy of model fit can be measured by the correlation coefficient (R^2). The R^2 value reflects how well the model fits the given data and is expressed as a value between 0 and 1 (0–100%). For the model developed in this experiment, the R^2 values for slump spread, T500, and gap passage values were 87%, 78% and 44%, respectively.

Table 6. Model confirmation.

Parameters	Responses		
	Slump Expansion (cm)	Gap Passing Value (cm)	T500 (s)
Std.Dev.	4.1	2.2	1.5
Mean	66.6	3.4	2.9
C.V.%	6.2	66.1	52.5
PRESS	1227.6	258.0	172.4
−2Log Likelihood	143.2	115.0	85.2
R2	0.87	0.44	0.78
Adj.R2	0.75	0.13	0.57
Pred.R2	0.34	−0.60	−0.16
Adeq. Precision	9.2	5.6	7.2
BIC	193.7	152.2	135.7
AIC	210.2	152.7	152.1

It can be seen that for slump spread and T500, the higher R^2 values indicate that the model has a better prediction accuracy. And the gap passing value R^2 is even lower than 50%, indicating a small fitting accuracy. In addition, the value of precision is the ratio of effective signal to noise, and a precision value greater than 4 is considered reasonable. As can be seen from Table 6, the precision values of all the models are greater than 4. This indicates that the predicted response accuracy of the model meets the requirements.

4. Discussion

In order to more intuitively reflect the relationship between the effects of N/B, W/B, and nanomaterial doping on SCGC workability indexes, Equations (2)–(4) were applied to plot the three-dimensional response surface plots and two-dimensional contour plots of the two-by-two interactions of the response factors; e.g., when plotting the response surface plots of the NS-NC interactions affecting the collapsed extensibility, replacing C in Equations with x, and D with y, and taking A and B as N/B to an intermediate value of 4.5% and W/B to an intermediate value of 0.55, respectively. The formulas were added to the Origin matrix to obtain a 3D response surface plot and a 2D contour plot of the NS-NC interaction. Therefore, the values of N/B and W/B in the response surface plots for the

NS-NC interaction are fixed at 4.5% and 0.55, respectively, and similarly the values of NS and NC doping in the response surface plots for the N/B-W/B interaction are fixed at 0.2%.

4.1. Interactive Effect of Nanomodification on the Working Performance of SCGCs
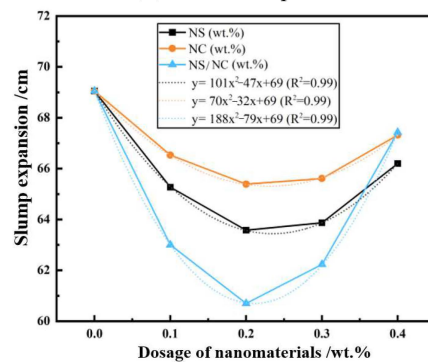
4.1.1. Effect of NS-NC on Slump Extensibility

The interaction effect of the nanomodified materials on the SCGC slump extensibility is shown in Figure 3, from which it can be seen in Figure 3a,b that the extensibility is larger when both NS and NC doping are at the end of the range; 0% NC vs. 0% NS, 0% NS vs. 0.4% NC, 0.4% NS vs. 0.4% NC, and 0.4% NS vs. 0% NC corresponds to an extensibility of about 67.5 cm. From Figure 3c, it can be more intuitively seen that the single doping of NS and NC decreases the slump extensibility of SCGC, and there is a small increase in the slump extensibility at a single doping level of 0.4%. It is worth noting that single doping of equal amounts of NS reduces the slump spread of SCGC to a greater extent compared to NC. This is due to the fact that NS provides soluble silica in a more alkaline environment, which corresponds to an increase in the modulus of the exciter [26] and promotes the formation of gel products.
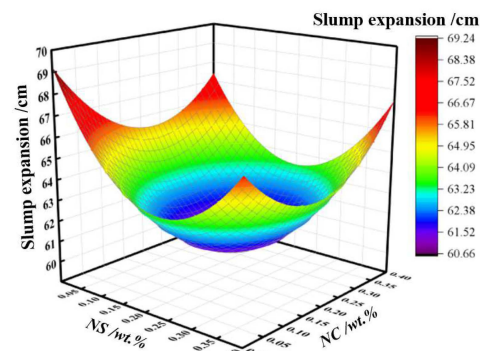
(**a**) 3D response surface plot
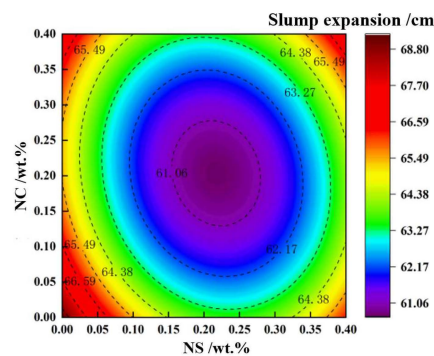
(**b**) 2D contour plot

(**c**) Effect of single/composite doping of nanomaterials

Figure 3. Interactive effect of nanomaterial doping on slump extensibility.

At the same time, there is an increase in silicon content in the liquid phase, increasing the unsaturation of Ca^{2+}, Al^{3+}, and other ions in the liquid phase [27] and promoting the participation of Ca and Al in raw materials such as BFS, FA, etc., in the geopolymerization reaction. In addition, a portion of the NS plays a role in nanofilling [28], which improves the stacking density of the slurry, increases the specific surface area, and reduces the degree of slump spread of the SCGC. While NC played the role of a nucleation site, its adsorption of Ca^{2+} promoted the formation of gel products such as C-A-S-H and C-(N)-A-S-H in the liquid phase in the BFS-FA composite alkali excitation system and optimized the gel structure [28]. Also, NC functioned as a group of nanofiller particles [29].

The higher doping (0.4%) of NS produced an excess of soluble silica inhibiting the reaction of Si in the gelling material, while the presence of excess NC hindered further polymerization of the gel products due to its low activity. It can be observed from Figure 3c that equal compounding of less than 0.35% of NS and NC further reduces the slump extensibility. The complex doping of the nanomaterials for 0.4% resulted in a substantial increase in the degree of extension, but it was still less than the value at zero doping. The minimum extension of 60.67 cm was obtained with the NC doping of 0.2% and NS doping of 0.22%. When the dosage was less than 0.2%, the composite addition of NS and NC significantly increased the magnitude of slump extensibility variation with dosage. This is due to the equimolar complexation of small amounts of NS and NC, and the small amount of soluble silicon provided by NS, which affects the unsaturation of ions in the liquid phase, and acts as a group of nanomicroagglomerates. In addition, the synergistic effect of the two nanomaterials then fully utilizes the large specific surface area of the particles, which further reduces the mobility of SCGC [30]. Similar conclusions were obtained in Li's study, where the synergistic effect of the particle-filling effect of nano-Al_2O_3 with the chemically active effect of nano-SiO_2 yielded the densest matrix [31,32].

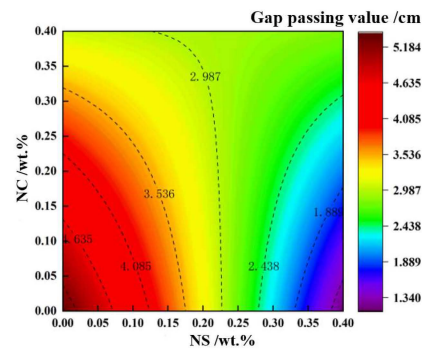### 4.1.2. Effect of NS-NC on Gap Passing Values

The interaction effect of the nanomodified materials on the gap passage values of SCGC is shown in Figure 4, where it can be seen that when NC doping is in the range of 0–0.3%, the gap passage value decreases more significantly with the increase in NS doping. The most significant of these was when the NC doping was 0. The gap passage value for NS doping of 0.4% was reduced by 4.25 cm compared to the doping of 0. And when the NC doping is higher than 0.3%, the gap passage value of SCGC is almost unchanged with the increase in compounded NS regardless of the NS doping. This is due to the fact that a small amount of NC particles do not fully function as nanofillers and will also disperse the precursor particles to some extent. At this point, the complex doping of NS significantly affects the SiO_2/Na_2O in the liquid phase environment, and the interstitial passage value of SCGC decreases significantly with the increase in NS composite doping. When the NC doping is larger, the adsorption of NC for Ca^{2+} fully plays the role of its nucleation site, so that there is more C-A-S-H gel polymerization in the liquid phase environment, on which the effect of compound doping of NS on the gap passage value is smaller.

From Figure 4c, it can be seen more intuitively that the gap passage value of SCGC decreases with the increase in nanomaterial doping, both for single- and complex-doped nanomodified materials. Compared to NC, the single doping of equal amounts of NS will reduce the SCGC gap passage value to a greater extent. This is in agreement with the findings of GAO X et al. [33]. With the increasing amount of single-doped nanomaterials, the decrease in the gap passage value is greater than the slump extension, and the gap passage value continues to decrease with increasing amount, with no tendency to increase at higher amounts. This indicates that the decreasing trend in the SCGC gap passage values with the increasing doping of single-doped nanomaterials is almost independent of the change in slump spread. It is noteworthy that the gap passage value decreases rapidly with increasing doping when compounding less than 0.2% of nanomaterials. When compounded with more than 2% of nanomodified materials, the increase in doping hardly decreases the gap passage value, and the gap passage value also increases slightly when

the doping is increased to 0.4% and is larger than the value when NS is doped alone. The reason for this is that the synergistic effect of NS and NC as nanomodified materials is optimized when about 0.2% of nanomaterials are added, and at this level of doping, the role of NC as a nucleation point for gels in the liquid phase is more consistent with the role of NS in promoting the participation of precursor particles in the reaction. A further equal increase in NS and NC doping does not reduce the gap passage value.
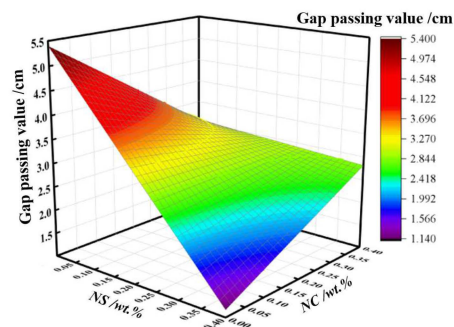
(**a**) 3D response surface plot

(**b**) 2D contour plot
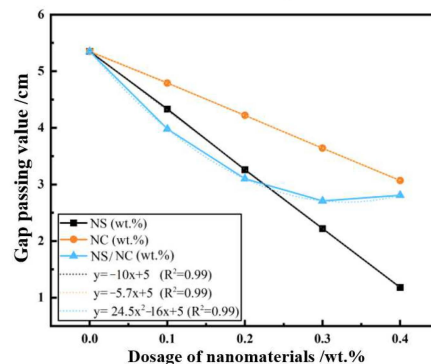
(**c**) Effect of single/composite doping of nanomaterials

Figure 4. Interaction effect of nanomaterial doping on gap passage values.

4.1.3. Impact of NS-NC on the T500

The effects of the NS admixture and NC admixture interaction on SCGC T500 are shown in Figure 5; when the NS admixture is 0–0.05% and 0.35–0.4%, the T500 of fresh concrete both increase almost linearly with the increase in NC admixture. When the NS admixture is 0.4%, as the NC admixture increases from 0% to 0.4%, the T500 increases from 1.13 s to 1.95 s, and the corresponding contour plots are diagonally linear. This is due to the fact that NC, as a nanoscale-modified material in SCGC, which itself is acting as a microaggregate filler, reduces the pores between precursor particles [34] and gel products, and at the same time, promotes the formation of gel products in the liquid phase, which reduces the mobility of SCGC and increases the T500. In the present experimental range,

the minimum T500 with a value of 0.95 s was obtained when both NC and NS doping were zero, and the maximum T500 with a value of 3.16 s was obtained when NS doping was 0.21% and NC doping was 0.35%.
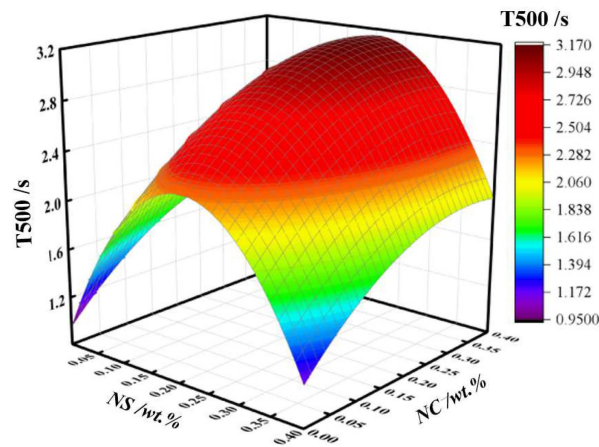
(**a**) 3D response surface plot
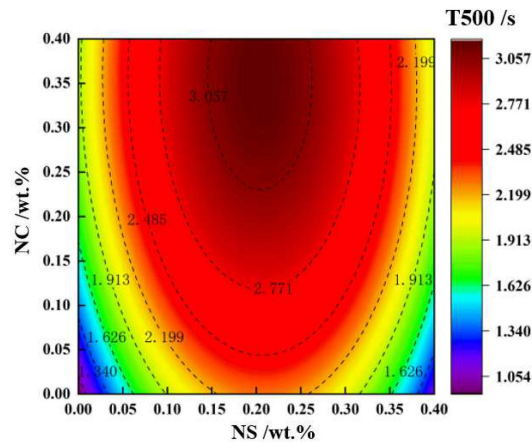
(**b**) 2D contour plot
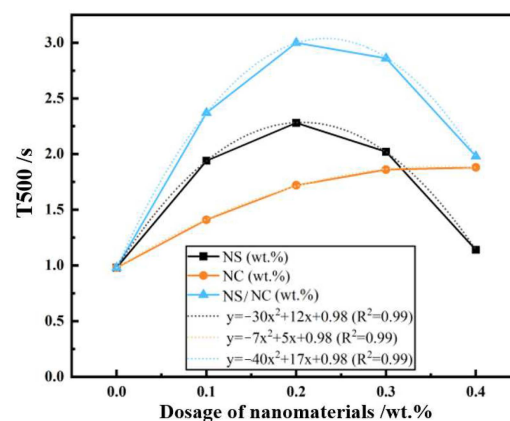
(**c**) Effect of single/composite doping of nanomaterials

Figure 5. Interaction effect of nanomaterial doping on T500.

From Figure 5c, it can be seen that regardless of which level the NC doping is at, T500 increases and then decreases with the increase in NS doping, and the corresponding contour plots are of a parabolic type. In addition, compared to the experimental group with NS alone, compounding NC on top of this increases the T500 of the freshly mixed slurry.

This suggests that excess NS reduces the unsaturation of Si in the reaction environment and inhibits the extent of precursor participation in the reaction.

4.1.4. Effect of Single/Multiple Doping of NS and NC on Rheological Properties

The static yield stress is the limiting shear stress that causes flow to begin to occur in SCGC, while the dynamic yield stress is the minimum shear stress that maintains the flow state of SCGC, and the plastic viscosity reflects the internal frictional resistance within the fluid that resists flow.

The effect of the single/composite doping of NS and NC on the rheological properties of SCGC is shown in Figure 6, and it can be seen from Figure 6a that compounding equal amounts of nanomodified materials leads to a small reduction in the static yield stress; this is especially so in the case of compounding 0.4% of nanomaterials, as the static yield stress is reduced to 124 Pa which is about 50 Pa different from the value of the static yield stress in the case of single doping of nanomaterials. It can be seen that the static yield stress of freshly mixed SCGC decreases when comparable amounts of NS and NC are compounded, whereas the single doping of nanomaterials significantly increases the static yield stress of SCGC. This is the reason why the gap passage values of complex-doped small amounts of nanomaterials SCGC are significantly smaller than those of single-doped NS.

From Figure 6b, it can be seen that unlike the effect on static yield stress, the increase in NC doping decreases the dynamic yield stress of SCGC. The reason is that the solubility of NC in an alkaline solution is lower than that of NS, which participates in the reaction to a lesser extent, and the addition of spherical NC particles also produces a spherical effect, which improves the dispersion of precursor particles and thus reduces the dynamic yield stress, which is similar to the role of the effect of NC on the fluidity properties of the matrix of ultrahigh-strength concrete, as shown in the study by Li [35]. Previous results have shown that NC mainly acts as an inert filler material, contributing to the production of denser microstructures and accelerating the reaction process of the cementitious materials through the boundary nucleation growth effect [36]. This is consistent with the single-doped NC corresponding to the largest slump spread law in Figure 3c.

From Figure 6c, it can be seen that the single doping of NC significantly reduces the plastic viscosity of SCGC compared to single doping of NS. The complex doping of NS and NC further reduces the plastic viscosity of SCGC. Combined with Figure 6b, it can be seen that the dynamic yield stress decreases with the increase in NC doping, which is related to the fact that NC doping significantly reduces the plastic viscosity of SCGC.
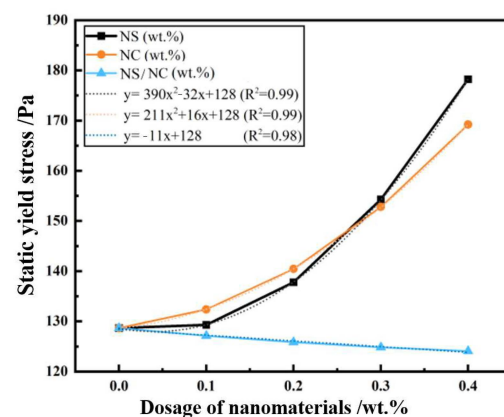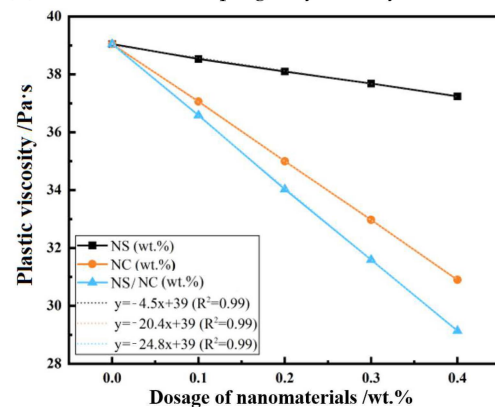

(**a**) Nanomaterial doping—static yield stress

Figure 6. *Cont.*
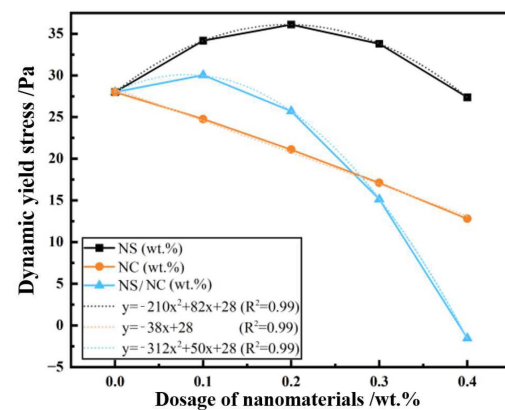
(**b**) Nanomaterial doping—dynamic yield stress

(**c**) Nanomaterial doping—plastic viscosity

Figure 6. Effect of single/composite doping of nanomaterials on rheological properties.

### 4.2. Interactive Effects of N/B and W/B on SCGC Operating Performance

4.2.1. Effect of N/B-W/B on Slump Extensibility

The effects of the N/B and W/B interactions on SCGC extensibility are shown in Figure 7. From Figure 7a,b, it can be seen that the slump extensibility of SCGC increased significantly with the increase in the W/B; when N/B was 4%, the extensibility increased from 55.7 cm to 78.7 cm when the W/B increased from 0.5 to 0.6, and when N/B was 4.45%, the extensibility increased from 51.3 cm to 71.4 cm when the W/B increased from. When N/B was 4.45%, the W/B increased from 0.5 to 0.6, and the extension increased from 51.3 cm to 71.4 cm. When N/B was 5%, the W/B increased from 0.5 to 0.6, and the extension increased from 60.5 cm to 77 cm; therefore, it can be seen that, even with a different N/B, the increase in the extension caused by the W/B is approximately the same, and the difference in the extension with the W/B between 0.5 and 0.6 is, in all, 20 cm or so. This indicates that the increase in W/B increases the slump spread of the SCGC almost equally. The increase in the W/B reduces the density of the slurry, disperses the aggregation and interaction between the gelling material and the nanomodified material, and reduces the degree of bonding between the aggregate and the slurry drop, which also weakens the particle-filling effect of the nanomaterials [37]. In addition, water is used as a carrier for alkali exciters in the geopolymerization reaction and is not required for the composition of the gel product [38,39]. Therefore, the increase in water content has a huge impact on GC fluidity [39]. The slump extensibility decreased firstly and then increased with the increase in N/B, and when N/B was greater than 4.3%, the slump extensibility increased with the increase in N/B. The corresponding contour plots are of a parabolic type. The reason for this is that the concentration of Na^+ and OH^- in the liquid phase environment increases with the increase in N/B, which leads to a more efficient excitation of the precursor particles by the exciter solution, which facilitates the polymerization and

generation of the gel products, such as C-A-S-H and N-A-S-H, and is macroscopically manifested as a decrease in the flow extension capacity [40]. It is worth noting that in the present study, in order to mitigate the fast-setting properties of alkali-excited slag geopolymer concrete, the N/B of SCGC was improved by incorporating Na_2CO_3 powder. The retardation effect of Na_2CO_3 is attributed to the reaction between Ca^{2+} dissolved from the BFS and $CO_3{}^{2-}$ from Na_2CO_3 in the liquid phase to form $CaCO_3$, which delays the dissolution of the BFS at moderate pH conditions [41]. Therefore, further increasing the N/B increases the collapse extension of the SCGC.
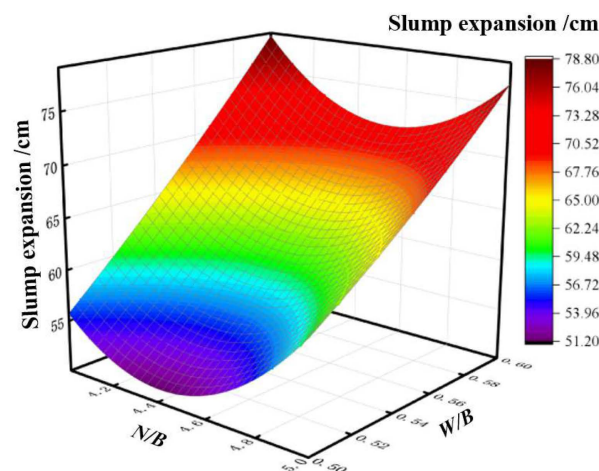
(**a**) 3D response surface plot
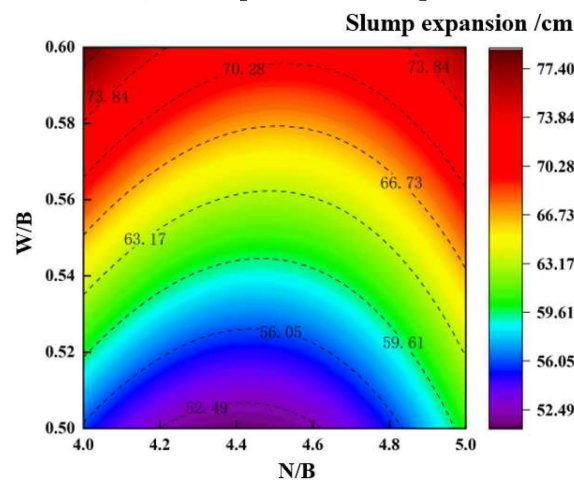
(**b**) 2D contour plot

Figure 7. N/B-W/B interaction effects on slump extensibility.

4.2.2. Effect of N/B-W/B on Gap Passing Values

The effect of N/B and W/B interaction on the SCGC gap passage value is shown in Figure 8. From Figure 8a,b, it can be seen that the gap passage value is the largest and the difference between the slump extensibility and the J-ring extensibility is 0.94 cm when the N/B is 5 while the W/B is 0.6. When the W/B takes the minimum value of 0.5, the difference between the SCGC slump extensibility and the J-ring extensibility is about 4.5 cm with almost no fluctuation regardless of N/B. At the same N/B, increasing the W/B can significantly increase the gap passage value of SCGC. This is due to the fact that the increase in the W/B disperses the precursor particles [42], inhibits the formation and further polymerization of the gel products, and makes the slurry structure looser. As a result, the difference between the slump extensibility and the J-ring extensibility decreases and the gap passage value of the SCGC increases. It is worth noting that as N/B increases,

the increase in clearance passage values from the increase in the W/B becomes greater. For example, when N/B is 4% and the W/B is increased from 0.5 to 0.6, the difference between slump spread and J-ring extension decreases from 4.52 cm to 2.47 cm, a decrease of 45.3%, while when N/B is 5% and the W/B is increased from 0.5 to 0.6, the difference between slump spread and J-ring extension decreases from 4.49 cm to 0.94 cm, a decrease of 79%. This is due to the fact that as N/B increases, the increase in Na_2CO_3 content has the effect of slowing down the coagulation, increasing the mobility of the SCGC, and improving the gap passage value of the SCGC.
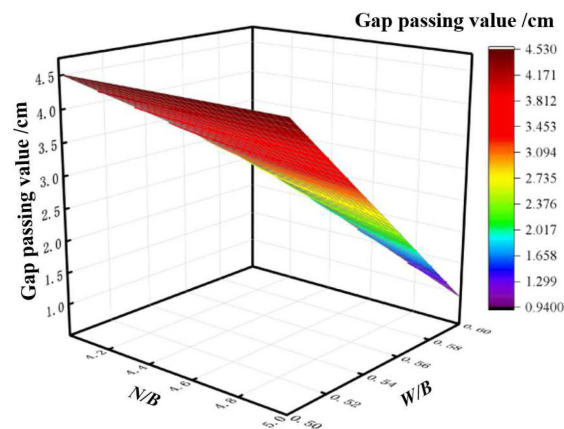
(**a**) 3D response surface plot
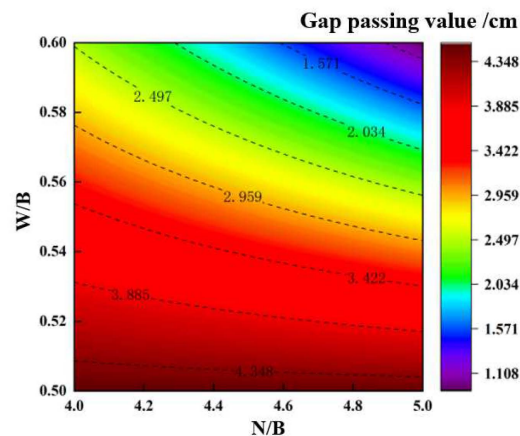
(**b**) 2D contour plot

Figure 8. N/B-W/B interaction effect on gap passing values.

4.2.3. Impact of N/B-W/B on the T500

The effects of the N/B and W/B interactions on SCGC T500 are shown in Figure 9, and it can be seen from Figure 9a,b, that with the increase in the W/B, the T500 decreases significantly. However, it is worth noting that the extent of the effect of the W/B on T500 diminishes as the N/B increases. For example, when the N/B is 5% and the W/B is increased from 0.5 to 0.6, T500 decreases from 5.27 s to 2.2 s, a decrease of 3.07 s. When the N/B is 4 and the W/B is increased from 0.5 to 0.6, T500 decreases from 8.24 s to 1.26 s, a decrease of 6.98 s, which is a decrease twice of that of the decrease when the N/B is 5%. It is thought that the high alkalinity of the environment promotes the dissolution of precursor particles and the formation of gel products as the N/B increases. On the other hand, the retardation effect of Na_2CO_3 weakened the effect brought by W/B on the flowability.
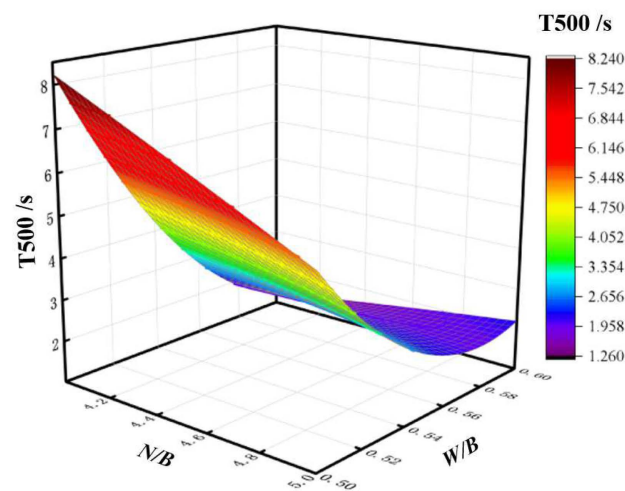
(**a**) 3D response surface plot
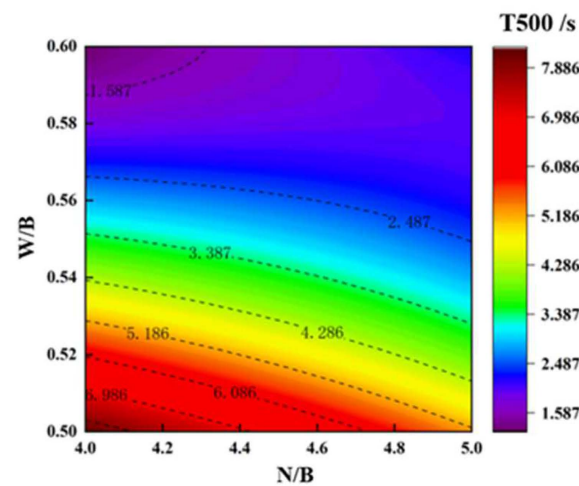
(**b**) 2D contour plot

Figure 9. N/B-W/B interaction on T500.

4.2.4. Combined Effect of N/B and W/B on Workability

When both NS doping and NC doping are 0.2% and the N/B is fixed at 4.5%, the effects of the W/B on the SCGC slump extensibility, gap passage value, and T500 are shown in Figure 10, from which the following can be seen: the extensibility of SCGC increases significantly with the increase in W/B, and the corresponding gap passage value decreases significantly. The trends in the gap passage value and slump spread were almost linear, which indicated that the increase in the W/B reduced the strength of the freshly mixed SCGC slurry structure and the diluted liquid phase reaction environment also weakened the role of the nucleation sites of the nanomodified materials; this in turn impeded the polymerization of the gel products, such as C-A-S-H and C-(N)-A-S-H, and the construction of the gel structure. It is noteworthy that the T500 of SCGC decreases significantly and then levels off with increasing W/B. This indicates that at a lower W/B (<0.55), the density of the SCGC slurry is relatively high, the bond strength of the slurry to the aggregate is higher, and the increase in the W/B significantly reduces the T500 of SCGC. However, an excessive W/B led to the segregation of SCGC, the weakening of the slurry-aggregate bonding, and a reduction in flowability. In addition, since water only acts as a carrier for the exciter solution during the geopolymerization reaction and not as a component of the gel product, excess water in SCGC is more likely to cause the segregation and deterioration of workability compared to cementitious materials.
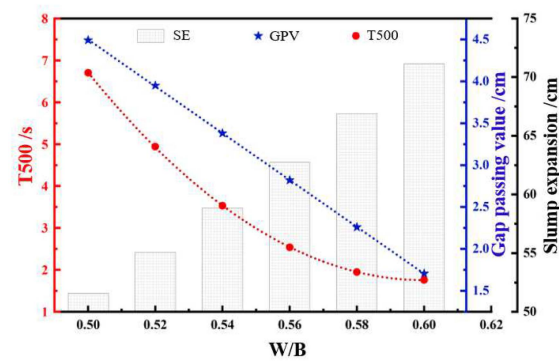
Figure 10. Effect of W/B on slump spread, gap passage value, and T500.

When both NS doping and NC doping are 0.2% and the W/B is fixed at 0.55, the effect of N/B on SCGC slump extensibility, gap passage value, and T500 is shown in Figure 11. It can be seen from the figure that the gap passing value and T500 of SCGC decreases with the increase in the N/B. However, the effect of the N/B changes on gap passing values and T500 within the scope of this test was much less than that of the W/B. The slump extensibility of SCGC decreased as the N/B was increased from 4% to 4.4%, and significantly increased when the N/B was further increased. This is due to the fact that 0.2% NS acts as a nanofilling component at lower alkaline environments with little change in the unsaturation of the reactive ions. This is due to the fact that as N/B increases, the alkalinity in the liquid phase environment is raised, and the concentration of OH^- in the liquid phase environment increases, which promotes the dissolution of Ca in the precursor particles and improves the C-A-S-H generation. When the alkali content was further increased, NS participated more in the geopolymerization reaction as soluble Si in the highly alkaline solution, and at the same time, the unsaturation of Si in the liquid phase environment was lowered, which contributed more to the excitatory effect of the excitant solution on the FA and the formation of more N-A-S-H gels, which have a lower chemical viscosity than C-A-S-H, and the NC adsorption of Ca^{2+} as nuclei used to polymerize C-A-S-H gels is less efficient. This leads to an increase in the slump spread of the SCGC.
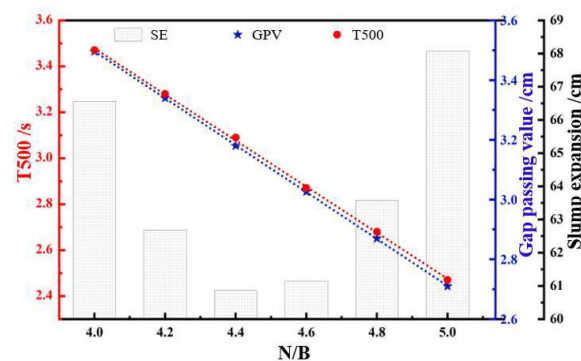

Figure 11. Effect of N/B on slump spread, gap passing value, and T500.

5. Conclusions

In this paper, the effect pattern of nanomaterials modification on the workability index of self-compacting geopolymer concrete (SCGC) was investigated, and the design of a Box–Behnken proportioning scheme and the interaction effect analysis among other factors was carried out based on the response surface methodology. Furthermore, the effects of nano-silica (NS), nano-calcium carbonate (NC), alkali content (N/B), and the water-cement ratio (W/B) on slump extensibility were quantitatively evaluated, as was T500 and the gap passage value; the differences in the modification effects caused by single and compounded

nanomodified materials were also discussed. Based on the above experimental results, the following conclusions can be drawn:

(1) The response surface methodology can systematically provide a proportioning scheme for the study of multi-factor response relationships and combine the experimental results for model construction and analysis. The quadratic multinomial equations fitted by the least squares method were obtained, the parameters of the slump spread, T500, and gap passing value were obtained from the quadratic fitting model, and the results of the significance test showed that the model's response prediction accuracy meets the requirements.

(2) The incorporation of NS and NC decreases the slump extensibility of SCGC, and there is a small increase in slump extensibility when it is higher than when 0.25% of the nanomaterials are incorporated, but the extensibility still decreases in comparison to the extensibility when no nanomaterials are incorporated. Compared to NC, the single doping of equal amounts of NS will reduce the slump spread of SCGC to a greater extent. The compounding of NS and NC significantly increased the magnitude of slump extensibility variation with dosage. T500 increases and then decreases with the increase in NS doping, and the corresponding contour plot is parabolic, which echoes the change rule of slump spread.

(3) The gap passage value of SCGC decreases with the increase in nanomaterial doping, both for single- and complex-doped nanomodified materials. In contrast, the gap passage value decreases rapidly with increasing doping when nanomaterials that constitute less than 0.2% are doped. When the nanomaterials are co-doped with more than 2% of nanomodified materials, the increase in doping hardly decreases the gap passage value and is greater than the value when NS is doped alone. It is noteworthy that the decreasing trend in SCGC gap passage values with the increasing doping of single-doped nanomaterials is almost independent of the change in slump spread.

(4) A W/B above 0.53 significantly increases the fluidity and decreases the T500 and clearance pass values of SCGC. It is worth noting that the formation of the gel product does not consume water, since water only acts as a carrier for the alkali exciter during the geopolymerization reaction. Therefore, excess water in SCGC is highly susceptible to segregation and the deterioration of the workability of concrete.

(5) The increase in the N/B diminishes the T500 and clearance pass values of the SCGC. The slump extensibility of SCGC decreased as the N/B was increased from 4% to 4.4%, and significantly increased when N/B was further increased. The effect of alkalinity change in the liquid phase on the release of soluble silica by NS doping needs to be fully considered; at the same time, excessive OH^- will lead to the formation of $Ca(OH)_2$ thin layer and Al-Si gel precipitation on the surfaces of BFS particles and FA particles, which is unfavorable for the full reaction of precursor particles.

(6) In this study, the response factors for SCGC obtain a better workability range with a W/B of (0.52–0.54), an N/B of (4.5–5%), NS constituting (0.05–0.15%), and NC constituting (0.25–0.35%). In addition, compared with the equal amounts of compound-doped nanomaterials, the differential compound-doped NS and NC can play a better role in optimizing the working performance of SCGC.

Author Contributions: Conceptualization, L.L.; Methodology, T.L.; Investigation, J.-C.T.; Data curation, Y.-H.T.; Writing—original draft, Y.-H.T., J.-C.T. and L.L. All authors have read and agreed to the published version of the manuscript.

Data Availability Statement: The original contributions presented in the study are included in the article, further inquiries can be directed to the corresponding author.

References

1. Singh, K. Experimental study on metakolin and baggashe ash based geopolymer concrete. *Mater. Today Proc.* **2021**, *37*, 3289–3295. [CrossRef]
2. Chen, Y.L.; Tong, J.Z.; Li, Q.H.; Xu, S.; Shen, L. Application of high-performance cementitious composites in steel–concrete composite bridge deck systems: A review. *J. Intell. Constr.* **2024**, *2*, 9180012. [CrossRef]
3. Li, Z.M.; Delsaute, B.; Lu, T.S.; Kostiuchenko, A.; Staquet, S.; Ye, G. A comparative study on the mechanical properties, autogenous shrinkage and cracking proneness of alkali-activated concrete and ordinary Portland cement concrete. *Constr. Build. Mater.* **2021**, *292*, 123418. [CrossRef]
4. Xue, C.H.; Sirivivatnanon, V.; Nezhad, A.; Zhao, Q. Comparisons of alkali-activated binder concrete (ABC) with OPC concrete-A review. *Cem. Concr. Compos.* **2023**, *135*, 104851. [CrossRef]
5. Pu, B.C.; Liu, B.; Li, L.; Pang, W.; Wan, Z. Influence of polypropylene fiber factor on flowability and mechanical properties of self-compacting geopolymer. *Materials* **2021**, *14*, 5025. [CrossRef]
6. Li, Z.J.; Liu, X.; Zhao, C.Y.; Wang, C.; Tian, X. Pore structure and mechanical properties of steel fiber reinforced geopolymer recycled aggregate concrete. *Acta Mater. Compos. Sin.* **2024**, *41*, 5383–5393.
7. Shaikh, F.U.A.; Hosan, A. Mechanical properties of steel fiber reinforced geopolymer concretes at elevated temperatures. *Constr. Build. Mater.* **2016**, *114*, 15–28. [CrossRef]
8. Ganesan, N.; Abraham, R.; Raj, S.D. Durability characteristics of steel fiber reinforced geopolymer concrete. *Constr. Build. Mater.* **2015**, *93*, 471–476. [CrossRef]
9. Liu, Y.W.; Shi, C.J.; Zhang, Z.H.; Li, N.; Shi, D. Mechanical and fracture properties of ultrahigh performance geopolymer concrete: Effects of steel fiber and silica fume. *Cem. Concr. Compos.* **2020**, *112*, 103665. [CrossRef]
10. Su, H.Z.; Xu, X.Y.; Zuo, S.L.; Zhang, S.; Yan, X. Research progress in monitoring hydraulic concrete damage based on acoustic emission. *J. Intell. Constr.* **2023**, *1*, 9180024. [CrossRef]
11. Palacios, M.; Puertas, F. Effect of superplasticizer and shrinkage-reducing admixtures on alkali-activated slag pastes and mortars. *Cem. Concr. Res.* **2005**, *35*, 1358–1367. [CrossRef]
12. Yang, L.; Zhu, Z.D.; Zhang, D.W.; Sun, H.; Huo, W.; Zhang, J.; Wan, Y.; Zhang, C. Influence mechanism of Nano-SiO$_2$ on geopolymer recycled concrete: Change mechanism of the microstructure and the anti-carbonation mechanism. *Cem. Concr. Compos.* **2024**, *146*, 105364. [CrossRef]
13. Yorulmaz, H.; Uzal, B.; Karahan, O.; Durak, U.; İlkentapar, S.; Atiş, C.D. Effect of nanoSiO$_2$ on strength and hydration characteristics of ternary cementitious systems. *Arab. J. Sci. Eng.* **2023**, *48*, 13649–13660. [CrossRef]
14. Ahmed, H.U.; Mohammed, A.S.; Faraj, R.H.; Qaidi, S.M.; Mohammed, A.A. Compressive strength of geopolymer concrete modified with nano-silica: Experimental and modeling investigations. *Case Stud. Constr. Mater.* **2022**, *16*, e01036. [CrossRef]
15. Durak, U.; Karahan, O.; Uzal, B.; İlkentapar, S.; Atiş, C.D. Influence of nano SiO$_2$ and nano CaCO$_3$ particles on strength, workability, and microstructural properties of fly ash-based geopolymer. *Struct. Concr.* **2021**, *22*, E352–E367. [CrossRef]
16. Zhang, P.; Wan, J.Y.; Wang, K.J.; Li, Q. Influence of nano-SiO$_2$ on properties of fresh and hardened high performance concrete: A state-of-the-art review. *Constr. Build. Mater.* **2017**, *148*, 648–658. [CrossRef]
17. Massana, J.; Reyes, E.; Bernal, J.; León, N.; Sánchez-Espinosa, E. Influence of nano- and micro-silica additions on the durability of a high-performance self-compacting concrete. *Constr. Build. Mater.* **2018**, *165*, 93–103. [CrossRef]
18. Zhu, Y.; Yang, Y.Z.; Yao, Y. Use of slag to improve mechanical properties of engineered cementitious composites (ECCs) with high volumes of fly ash. *Constr. Build. Mater.* **2012**, *36*, 1076–1081. [CrossRef]
19. Nuaklong, P.; Sata, V.; Wongsa, A.; Srinavin, K.; Chindaprasirt, P. Recycled aggregate high calcium fly ash geopolymer concrete with inclusion of OPC and nano-SiO$_2$. *Constr. Build. Mater.* **2018**, *174*, 244–252. [CrossRef]
20. Deb, P.S.; Sarker, P.K.; Barbhuiya, S. Sorptivity and acid resistance of ambient-cured geopolymer mortars containing nano-silica. *Cem. Concr. Compos.* **2016**, *72*, 235–245. [CrossRef]
21. Ali, L.; Ouni, M.H.E.; Raza, A.; Janjua, S.; Ahmad, Z.; Ali, B.; Kahla, N.B.; Bai, Y. Experimental investigation on the mechanical and fracture evaluation of carbon Fiber-Reinforced cementitious composites with Nano-Calcium carbonate. *Constr. Build. Mater.* **2021**, *308*, 125095. [CrossRef]
22. Sun, X.J.; Wang, S.Q.; Jin, J.P.; Wang, Z.; Gong, F. Computational methods of mass transport in concrete under stress and crack conditions: A review. *J. Intell. Constr.* **2023**, *1*, 9180015. [CrossRef]

23. Feng, J.H.; Yang, F.; Qian, S.Z. Improving the bond between polypropylene fiber and cement matrix by nano calcium carbonate modification. *Constr. Build. Mater.* **2021**, *269*, 121249. [CrossRef]

24. Liu, Z.H.; Liu, J.F.; Cui, C.; Zhang, T.R. Experimental study on optimization of binary solid waste geopolymer ratios based on response surface methodology. *Mater. Rep.* **2023**, *38*, 24100011.

25. *JGJ/T 283-2012*; Technical Specification for Application of Self-Compacting Concrete. Ministry of Housing and Urban-Rural Development: Beijing, China, 2012.

26. Li, L.; Wei, Y.J.; Li, Z.L.; Farooqi, M.U. Rheological and viscoelastic characterizations of fly ash/slag/silica fume-based geopolymer. *J. Clean. Prod.* **2022**, *354*, 131629. [CrossRef]

27. Ravikumar, D.; Neithalath, N. Reaction kinetics in sodium silicate powder and liquid activated slag binders evaluated using isothermal calorimetry. *Thermochim. Acta* **2012**, *546*, 32–43. [CrossRef]

28. Sumesh, M.; Alengaram, U.J.; Jumaat, M.Z.; Mo, K.H.; Alnahhal, M.F. Incorporation of nano-materials in cement composite and geopolymer based paste and mortar—A review. *Constr. Build. Mater.* **2017**, *148*, 62–84. [CrossRef]

29. Xu, H.; Van Deventer, J.S.J. Geopolymerisation of multiple minerals. *Miner. Eng.* **2002**, *15*, 1131–1139. [CrossRef]

30. Ye, J.Y.; Zhang, W.S. Research progress of nano-modified alkali-inspired cementitious materials. *J. Chin. Ceram. Soc.* **2020**, *48*, 1263–1277.

31. Nazari, A.; Sanjayyan, J.G. Hybrid effects of alumina and silica nanoparticles on water absorption of geopolymers: Application of Taguchi approach. *Measurement* **2015**, *60*, 240–246. [CrossRef]

32. Guo, X.; Shi, H.; Wei, X. Pore properties, inner chemical environment, and microstructure of nano-modified CFA-WBP (class C fly ash-waste brick powder) based Geopolymers. *Cem. Concr. Compos.* **2017**, *79*, 53–61. [CrossRef]

33. Gao, X.; Yu, Q.L.; Brouwers, H.J.H. Characterization of alkali activated slag–fly ash blends containing nano-silica. *Constr. Build. Mater.* **2015**, *98*, 397–406. [CrossRef]

34. Péra, J.; Husson, S.; Guilhot, B. Influence of finely ground limestone on cement hydration. *Cem. Concr. Compos.* **1999**, *21*, 99–105. [CrossRef]

35. Kawashima, S.; Seo, J.-W.T.; Corr, D.; Hersam, M.C.; Shah, S.P. Dispersion of $CaCO_3$ nanoparticles by sonication and surfactant treatment for application in fly ash–cement systems. *Mater. Struct.* **2014**, *47*, 1011–1023. [CrossRef]

36. Li, W.G.; Huan, Z.Y.; Cao, F.L.; Sun, Z.; Shah, S.P. Effects of nano-silica and nano-limestone on flowability and mechanical properties of ultra-high-performance concrete matrix. *Constr. Build. Mater.* **2015**, *95*, 366–374. [CrossRef]

37. Huang, Y.; Hu, X.; Shi, C.J.; Wu, Z.M. A review of the formation and improvement of the transition zone at the cement paste-aggregate interface in concrete. *Mater. Rep.* **2023**, *37*, 106–117.

38. Škvára, F.; Kopecký, L.; Šmilauer, V.; Bittnar, Z. Material and structural characterization of alkali activated low-calcium brown coal fly ash. *J. Hazard.* **2009**, *168*, 711–720. [CrossRef]

39. Xu, H.; Van Deventer, J.S.J. The effect of alkali metals on the formation of geopolymeric gels from alkali-feldspars. *Colloid Surf. A* **2003**, *216*, 27–44. [CrossRef]

40. Sun, B.B.; Sun, Y.B.; Ye, G.; De Schutter, G. A mix design methodology of blast furnace slag and fly ash-based alkali-activated concrete. *Cem. Concr. Compos.* **2023**, *140*, 105076. [CrossRef]

41. Chen, Y.N.; Xia, K.L.; Jia, Z.J.; Gao, Y.; Zhang, Z.; Zhang, Y. Extending applicability of 3D-printable geopolymer to large-scale printing scenario via combination of sodium carbonate and nano-silica. *Cem. Concr. Compos.* **2024**, *145*, 105322. [CrossRef]

42. Sun, B.B.; Sun, Y.B.; Ye, G.; De Schutter, G. A mix design methodology of slag and fly ash-based alkali-activated paste. *Cem. Concr. Compos.* **2022**, *126*, 104368. [CrossRef]